Volume 9 | Number 23 | 21 June 2017 | Pages 7689–8034

Nanoscale

rsc.li/nanoscale

ISSN 2040-3372

ROYAL SOCIETY OF CHEMISTRY

PAPER

Emily D. Cranston, Jose M. Moran-Mirabal *et al.*

Beyond buckling: humidity-independent measurement of the mechanical properties of green nanobiocomposite films

NCNST

Nanoscale

PAPER

View Article Online
View Journal | View Issue

Cite this: *Nanoscale*, 2017, **9**, 7781

Beyond buckling: humidity-independent measurement of the mechanical properties of green nanobiocomposite films†

Urooj Gill,[a] Travis Sutherland,[a] Sebastian Himbert,[b] Yujie Zhu,[a] Maikel C. Rheinstädter,[b] Emily D. Cranston*[c] and Jose M. Moran-Mirabal*[a]

Received 11th January 2017,
Accepted 27th March 2017

DOI: 10.1039/c7nr00251c

rsc.li/nanoscale

Precise knowledge of the mechanical properties of emerging nanomaterials and nanocomposites is crucial to match their performance with suitable applications. While methods to characterize mechanical properties exist, they are limited by instrument sensitivity and sample requirements. For bio-based nanomaterials this challenge is exacerbated by the extreme dependence of mechanical properties on humidity. This work presents an alternative approach, based on polymer shrinking-induced wrinkling mechanics, to determine the elastic modulus of nanobiocomposite films in a humidity-independent manner. Layer-by-layer (LbL) films containing cellulose nanocrystals (CNCs) and water-soluble polymers were deposited onto pre-stressed polystyrene substrates followed by thermal shrinking, which wrinkled the films to give them characteristic topographies. Three deposition parameters were varied during LbL assembly: (1) polymer type (xyloglucan – XG, or polyethyleneimine – PEI); (2) polymer concentration (0.1 or 1 wt%); and (3) number of deposition cycles, resulting in 10–600 nm thick nanobiocomposite films with tuneable compositions. Fast Fourier transform analysis on electron microscopy images of the wrinkled films was used to calculate humidity-independent moduli of 70 ± 2 GPa for CNC-$XG_{0.1}$, 72 ± 2 GPa for CNC-$PEI_{0.1}$, and 32.2 ± 0.8 GPa for CNC-$PEI_{1.0}$ films. This structuring method is straightforward and amenable to a wide range of supported thin films.

Introduction

The unique chemical, electrical and mechanical properties of nanomaterials make them attractive for a diverse range of applications spanning nanomedicine, nanoelectronics and nanomachines. Current and future products incorporating nanomaterials include sensors, energy storage/conversion devices, wearable electronics, drug delivery systems, inks, and water purification systems, among many others.[1–4] The past 30 years have seen immense progress in the production of nanomaterials and devices and the development of nanocharacterization techniques. However, despite the importance of mechanical performance in many applications, methods to measure nanomechanical properties have failed to keep pace. This work thus presents a structuring method that allows for the humidity-independent determination of the elastic modulus of supported thin film nanocomposites, prepared from plant-derived nanoparticles and polymers that are assembled using a water-based layer-by-layer (LbL) deposition approach.

Current methods to determine the elastic modulus of nanocomposite thin films include nanoindentation, dynamic mechanical thermal analysis, three-point bending flexural tests, and buckling measurements.[5,6] However, these techniques are often limited by their precision, lacking the sensitivity required to detect the mechanical response of individual nanoparticles or ultrathin films. Furthermore, conventional mechanical testing methods, and even some nanomechanical techniques, are only amenable to free-standing films, but are incapable of handling films with sub-micron thicknesses. In all cases, sample preparation, technique operation and data processing can be highly nanomaterial specific. These problems are exacerbated when it comes to working with thin films that are sensitive to humidity, such as films fabricated from bio-based nanomaterials like crystallites and nanofibers.

Nanocellulose is a family of bio-based materials (*e.g.* cellulose nanocrystals – CNCs, and cellulose nanofibrils – CNFs) that strongly interact with water,[7] which has made it challen-

[a]*Department of Chemistry and Chemical Biology, McMaster University, 1280 Main St. W., Hamilton, ON, Canada, L8S 4M1. E-mail: moran-mirabal@mcmaster.ca*
[b]*Department of Physics and Astronomy, McMaster University, 1280 Main St. W., Hamilton, ON, Canada, L8S 4M1*
[c]*Department of Chemical Engineering, McMaster University, 1280 Main St. W., Hamilton, ON, Canada, L8S 4L7. E-mail: ecranst@mcmaster.ca*
†Electronic supplementary information (ESI) available: Supplementary figures. See DOI: 10.1039/c7nr00251c

ging to accurately quantify the mechanical properties of nanocellulose-containing composites.[8–10] Nanocellulose is a "green" and non-toxic[11] nanomaterial extracted from plants, algae, bacteria and tunicate with a broad range of applications. Favourable properties of nanocellulose include its high chemical, colloidal, and thermal stability (compared to other bio-based materials), large aspect ratio, and impressive mechanical strength resulting from cellulose's ability to form tightly packed crystalline structures.[12]

The elastic modulus of crystalline cellulose has been debated for decades based on X-ray diffraction, inelastic X-ray scattering, atomic force microscopy (AFM), Raman spectroscopy, and modeling techniques – all of which have their own assumptions and limitations. Despite conflicting results, the elastic modulus for crystalline cellulose is taken to be in the 57–220 GPa and 9–50 GPa range in the axial and transverse directions, respectively.[8,13] The mechanical properties of individual CNCs have also been assessed by AFM[14] and Raman spectroscopy,[15] where the axial modulus values ranged from 57–143 GPa.[8] The specific modulus of nanocellulose is thus comparable to materials such as Kevlar or steel[12] and is predicted to greatly reinforce matrix materials according to geometric percolation models.[16] However, to date these properties have not been fully exploited in nanobiocomposites, partially due to their humidity dependence.

In the present study, we have used an "extreme case" of the SIEBIMM (strain-induced elastic buckling instability for mechanical measurements) method[6,17] to irreversibly structure LbL CNC nanocomposite films, through the extensive compressive stress induced by the shrinkage of an underlying shape-memory polymer. We demonstrate that this structuring approach allows us to quantify the mechanical properties of the films in a humidity-independent manner. Films of CNCs and water-soluble polymers were deposited onto pre-stressed polystyrene (PS) substrates, after which the substrates were heated above their glass transition temperature and shrunken, causing wrinkling of the nanocomposite films. The PS shrinking method has been previously used to create micro- and nanostructured surfaces from metallic, oxide, and carbon nanotube thin films,[18–22] but has not been applied to structure or measure the modulus of nanobiocomposite films. In particular, the humidity independent nature of the modulus measurement strategy and irreversibility of the structures has not been previously shown.

The LbL nanocomposite films used in this study were prepared by dipping the PS substrate in alternating aqueous baths of CNCs and either the hemicellulose xyloglucan (XG) or the cationic polyelectrolyte polyethyleneimine (PEI), where the interactions responsible for layer build-up were van der Waals[23] and electrostatic interactions,[9,24] respectively. CNC-XG films are interesting as mimics for the plant cell wall, where XG is believed to crosslink individual cellulose microfibrils and increase the strength and load-bearing properties of the cell wall,[25] and have also been used as sensors for the detection of enzymes.[23,26–30] On the other hand, little work has focused on CNC-PEI mixtures and films, which represent model nanobiocomposite systems where the CNCs are strongly incorporated into the polymeric matrix through electrostatics. Previous SIEBIMM measurements on CNC-PEI films have reported elastic moduli of 16, 12, and 3.5 GPa at 30, 42, and 64% relative humidity,[9,10] demonstrating that the films' mechanical properties are highly humidity dependent. The complexity of equilibrating films under controlled humidity for long times and performing the measurements under identical conditions make it prohibitive to extensively test multiple nanobiocomposite formulations, which has led to the approach presented here.

In this work, three parameters were varied during LbL film assembly: polymer type, polymer concentration, and the number of deposition cycles, where the mechanical properties of these films were rapidly and accurately quantified, something that would have been difficult to achieve using the SIEBIMM approach. We have observed marked differences in the mechanical properties of the nanobiocomposite films based on the identity of the polymer used and its relative content within the film. We hypothesize that the differences observed stem from the different driving forces involved in the film assembly and the intrinsic polymer properties. Our results show that the rational use of polymer components can lead to films with tuneable stiffness and can extend the range of mechanical properties and surface topographies attainable with nanocellulose materials. We anticipate that these new nanobiocomposites will find applications in smart packaging, cell-based biosensors, extracellular matrix mimics, and tissue engineering substrates.

Experimental section

Chemicals

Deionized water with a resistivity of 18.2 MΩ cm was used for all experiments (Milli-Q A10 Purification System, Millipore, Etobicoke, Canada). Polyallylamine hydrochloride (PAH, M_w = 120 000–200 000 g mol^{-1}) was purchased from Polysciences (Warrington, PA) and prepared in water to a concentration of 0.1 wt%. A 3 wt% cellulose nanocrystal (CNC) suspension was obtained through acid hydrolysis of cotton filter aid (Whatman ashless filter aid, GE Healthcare Canada, Mississauga, Canada). A xyloglucan (XG) solution (0.1 wt%) was a gift from Dr Laurent Heux (CNRS, Grenoble, France). Polyethyleneimine (PEI, M_w = 750 000 g mol^{-1}, 50% (w/v) in water) was purchased from Sigma-Aldrich (Oakville, Canada), and prepared in water to concentrations of 0.1 wt% and 1 wt%.

Preparation of cellulose nanocrystals (CNCs)

CNCs were produced through the sulfuric acid hydrolysis of cotton, as reported previously.[31] A total of 700 mL sulfuric acid (64 wt%, Sigma Aldrich, Oakville, ON, Canada) was used to hydrolyze 40 g cotton filter aid in a 45 °C water bath for 45 minutes, with constant mechanical stirring. The reaction was quenched by diluting 10-fold in Milli-Q water and decanted. The mixture was repeatedly centrifuged in 10-minute

intervals at 5500*g* to remove excess acid. A stable CNC suspension was obtained, where no pellet formed following centrifugation. The suspension was then dialyzed against Milli-Q water for two weeks, until the pH of the external dialysis reservoir stabilized. Following this, a point probe sonicator (Sonifier 450, Branson Ultrasonics, Danbury, CT) was used to sonicate the CNC suspension in an ice water bath for 45 minutes, in three 15-minute intervals. The suspension was filtered through a glass microfiber filter (Whatman grade GF/B, VWR, Chicago, IL), yielding a solution of approximately 1 wt% CNCs. The CNC suspension was concentrated to 3 wt% through evaporation at ambient conditions, and its pH was adjusted from 3.36 to 6.07 using 10 M NaOH (EMD Millipore, Darmstadt, Germany), such that CNCs were used in the sodium-form. Sulfate half-ester content grafted to the CNCs was measured using conductometric titrations,[32] which showed that the sulfur content on the CNCs was 0.43 wt%, corresponding to 0.25 charge groups per nm^2. Dynamic light scattering (DLS) indicated that the average "apparent" size of the CNCs was 92 nm. By AFM, the average CNC dimensions were 197 nm in length and 8 nm in height.

Polystyrene (PS) substrate preparation

Pre-stressed PS shrink films (Graphix Shrink Film, Graphix, Maple Heights, OH) were used as substrates, and were first cut into 2 × 2 cm squares with a Robo Pro CE5000-40-CRP cutter (Graphtec America Inc., Irvine, CA). The CB15UB ceramic blade (Graphtec America Inc., Irvine, CA) was used with a force, quality and speed set of 30, 1, and 1, respectively. The square substrates were cleaned under orbital agitation (50 rpm) for 5 minutes each in isopropanol, ethanol, and water baths, consecutively, and dried using a nitrogen stream. Cleaned PS substrates were stored until ready to use.

Nanobiocomposite film preparation

Films were prepared on PS substrates using the LbL technique. PS substrates were first cleaned using air plasma at 600 mTorr for 3 minutes (PDC001 Expanded Plasma Cleaner, Harrick Plasma, Ithaca, NY). The clean substrates were then dipped into the following solutions/suspensions for 15 minutes each: (a) PAH, (b) CNCs (3 wt%), and (c) XG or PEI (0.1 wt% or 1 wt%). Following each dipping step, the PS substrates were rinsed in water for 5 minutes then dried using a nitrogen stream. After the initial PAH layer, the substrates were alternated between CNC suspensions and XG or PEI solutions. One bilayer ($N = 1$) was defined as a single deposition step of CNCs followed by an adsorption step with XG or PEI, and films were denoted CNC-XG or CNC-PEI; thus, integer bilayers had XG or PEI as the outermost layer and half-integer bilayers had CNCs as the top layer. Nanobiocomposite films were prepared from $N = 1$ to 20 bilayers for CNC-$XG_{0.1}$ films, and from $N = 1$ to 20.5 bilayers for CNC-$PEI_{0.1}$ ([PEI] = 0.1 wt%) and CNC-$PEI_{1.0}$ ([PEI] = 1 wt%) films.

Structuring of nanobiocomposite films

PS substrates with CNC-polymer films of varying thicknesses were shrunken in an isotemp vacuum oven (Fisher Scientific, Ottawa, ON, Canada) at 135 °C for 15 minutes, on aluminum boats lined with parchment paper.[18] These boats allowed for uniform heat transfer throughout the PS substrates, avoiding any distortion forming in the shrunken substrates.

Atomic force microscopy (AFM)

AFM images of structured CNC-$PEI_{1.0}$ films ($N = 20$ bilayers) were obtained in Alternating Current (AC) mode with a speed of 0.5 Hz, using an Asylum MFP-3D atomic force microscope (Asylum Research an Oxford Instrument Company, Santa Barbara, CA). Rectangular FMR cantilevers (NanoWorld) were used with normal spring constants of 1.2–5.5 N m^{-1} and resonant frequencies of 60–90 kHz.

Variable angle spectroscopic ellipsometry (VASE)

Thickness measurements were obtained for nanobiocomposite films prepared on Si substrates. A M-2000UI™ variable angle spectroscopic ellipsometer (J. A. Woollam Co., Inc., Lincoln, NE) was used, which spanned wavelengths of 250–1680 nm and angles from 55–75 degrees, in 5 degree increments, to obtain ellipsometric data for the films. The CompleteEASE® Software was used to extract the thickness values of the nanobiocomposite films. Here, the Cauchy model was used to fit the ellipsometric data with the assumption that transparent films were present on the Si substrates.

X-ray diffraction (XRD)

X-ray diffraction data was obtained using the Biological Large Angle Diffraction Experiment (BLADE) in the Laboratory for Membrane and Protein Dynamics at McMaster University. X-ray measurements were conducted at room temperature and ambient relative humidity using a Rigaku SmartLab X-ray diffractometer (Rigaku Corporation), which was equipped with a 9 kW (45 kV, 200 mA) CuKα rotating anode at a wavelength of 1.5418 Å. X-ray measurements were obtained for samples deposited on Si substrates, which consisted of pure CNCs, XG, PEI and samples that consisted of CNC-$XG_{0.1}$ and CNC-$PEI_{1.0}$ films ($N = 20$ bilayers) and CNC-$PEI_{0.1}$ films ($N = 40$ bilayers). Both the source and the detector were mounted on movable arms, and the wafers remained horizontal for the duration of the measurements. The wafers were oriented in the X-ray diffractometer such that the $q_{||}$-axis probed the lateral structure parallel to the wafer surface, and the out-of-plane structure, q_z, perpendicular to the substrate. Multi-layer optics were focused to give a high intensity beam parallel to the monochromatic X-ray intensities (up to 10^{10} counts per mm^2 per s), from which a sketch of the resulting scattering geometry was generated. Note that there was no risk of sample damage using this in-house technique, as a result of the large beam size and the relatively low intensity of the X-ray beam itself. A 2D intensity map was obtained from these XRD experiments using MATLAB, which showed the area of the reciprocal space. The

corresponding real-space length scales were 2.5–60 Å and were determined using the equation $d = \frac{2\pi}{|Q|}$, where d is the distance between two scatterers and Q is the scattering vector. The intensity maps were integrated over the azimuth and the meridian, and the resulting curves were fitted using a Lorentzian distribution. The diffraction patterns of the pure samples (CNC, XG and PEI) were fitted with multiple-peak profiles. These base profiles were then used to deconvolve the XRD data of the nanobiocomposite films into its individual components based on the relative weight of the profiles. Here, the signal intensity of the components was assumed to be directly correlated to their mass abundance in the nanobiocomposite films. We validated the method used to extract these film compositions by repeating the analysis on a drop-cast film of 50 : 50 CNC : $PEI_{1.0}$. The X-ray analysis for this film was performed as described above, where measurements were taken at 10% relative humidity due to the hygroscopic nature of the film components.

White light interference microscopy (WLIM)

WLIM measurements were taken using a Zygo NewView 5000 white light interferometer (Zygo Corporation, Middlefield, CT). Data was obtained for nanobiocomposite films formed on PS substrates, before and after shrinking. Five different areas on each substrate were imaged onto a charge coupled device (CCD) camera using a 50× objective with 2× additional optical zoom, resulting in fields of view of 70 × 50 μm, and a camera pixel size of 112 nm. The topographical maps obtained through WLIM were used to calculate the root mean square (RMS) roughness of each of the surveyed areas, from which an average RMS roughness value was calculated. For all images, a fast Fourier transform (FFT) band pass filter was applied to remove noise with cut-off frequencies of 183.35 mm^{-1} and 558.79 mm^{-1}. The MetroPro software (Zygo Corporation, Middlefield, CT) was used for image analysis.

Scanning electron microscopy (SEM)

SEM images were obtained for PS substrates with structured nanobiocomposite films using a JEOL JSM-7000S (JEOL USA, Inc., Peabody, MA) scanning electron microscope with an accelerating voltage of 2.5 kV, working distance of 6 mm, and low probe current of 30 μA.

Structure analysis of structured nanobiocomposite films

The characteristic wrinkle length (ζ) of the structured films was defined as the width of the resulting wrinkles, which is proportional to the persistence length (ξ) described by Groenewold,[33] and, like the persistence length, also shows a linear correlation to the film's thickness. The values for ζ at the different thicknesses and film compositions were calculated from the 2D FFT power spectra of the corresponding SEM images (Fig. S1†). SEM images taken at various magnifications were cropped into 900 × 900 pixel images and analyzed individually. Each image was adjusted for its brightness and contrast, after which the Canny threshold method on MATLAB was used to determine the edges of the wrinkled structures, which were rendered as a binary image. A MATLAB program was used to run a 2D FFT of the binary image. The power spectrum and the probability *vs.* length scale (μm) plots were generated from the binary image. The probability values were normalized to the maximum probability, then averaged for all SEM images and analyzed for each data point. A probability *vs.* log (length scale) plot was used to identify the values corresponding to the highest probability, which were averaged to determine the ζ of the structured films.

Elastic modulus calculations

To determine the elastic modulus of the nanobiocomposite films, plots of the characteristic wrinkle length (ζ) *vs.* film thickness (h) were generated. A linear regression to $\xi = a\zeta = 2\pi\eta^{2/3}h$, allowed us to extract the value for the parameter:

$$\eta = \frac{E_f(1-\nu_{PS}{}^2)}{3E_{PS}(1-\nu_f{}^2)} \quad (1)$$

where E_f, ν_f are the elastic modulus and Poisson's ratio for the rigid film and E_{PS}, ν_{PS} are the elastic modulus and Poisson's ratio for bulk polystyrene at 135 °C (the temperature at which the films were shrunken).[33,34] The scaling factor a was calibrated by using the reported modulus (70 GPa)[35,36] and Poisson's ratio (0.42)[36] for thin gold films deposited by sputtering (for full detail on the calibration, see ESI†). Values of E_{PS} = 1.63 GPa and ν_{PS} = 0.36 were used for the PS substrate at 135 °C in the calculations.[37] To obtain the final elastic moduli of the polymer-CNC nanobiocomposite films, a Poisson's ratio of 0.3 was used, which has been reported to match that of the cell wall material (hemicelluloses and cellulose)[38] and is intermediate to that reported for CNCs (0.28) and the polymers used in the formation of the nanobiocomposite films (0.33).[39]

Results and discussion

Structuring of CNC-polymer nanobiocomposite films

Nanobiocomposite films containing CNCs and a complementary polymer were prepared using the LbL method. The films were deposited onto pre-stressed PS substrates pretreated with a monolayer of poly(allylamine hydrochloride) (PAH), which is known to enhance the adsorption of the first layer of CNCs (Fig. 1a).[9] The LbL deposition process was entirely water-based, where the films were built to the desired thickness through the alternating adsorption of CNCs and either XG or PEI from dilute aqueous solutions. The prepared CNC-polymer films consisted of full (N) or half-integer bilayers (N + 0.5), where either polymer or CNCs (Fig. 1b) were the outermost layer, respectively. XG and PEI (Fig. 1c) were chosen as polymers for the LbL build-up of the nanobiocomposite films because they interact strongly with CNCs and have been previously shown to deposit as uniform coatings onto CNC layers.[9,23,26,28–30] Following LbL film build-up, the PS substrates were heated above their glass transition temperature and shrunken isotropically. This shrinking process generated compressive stress, which turned the smooth CNC-polymer

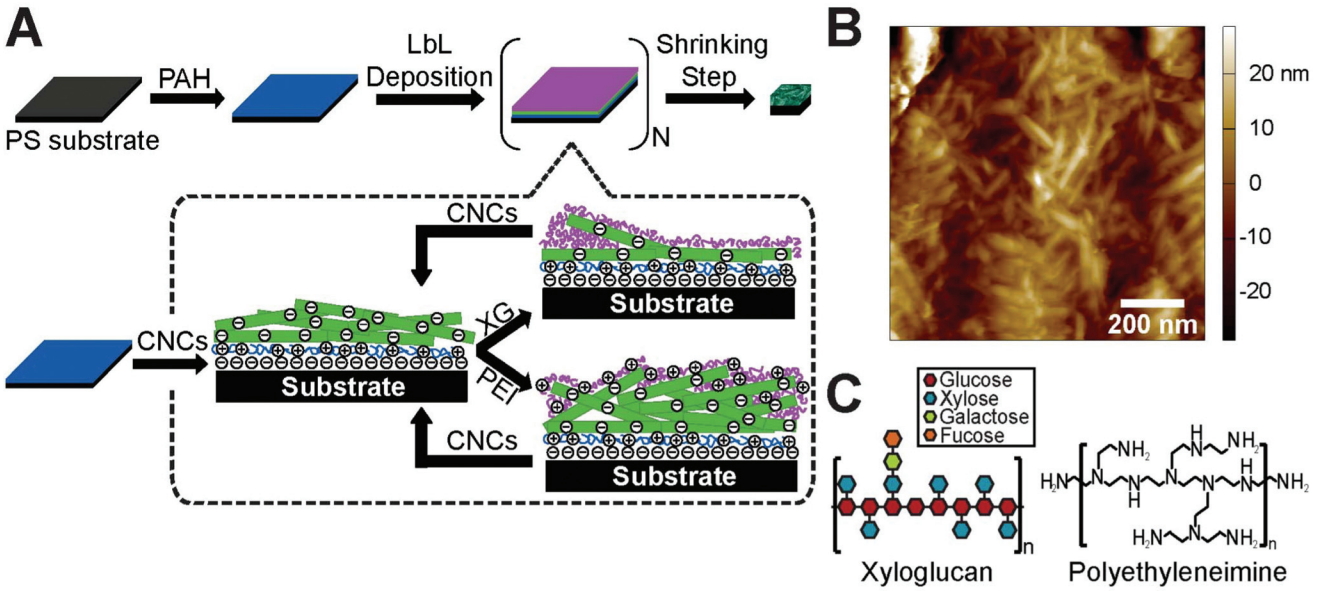

Fig. 1 Fabrication of LbL nanobiocomposite structured films. (a) LbL films were fabricated on pre-stressed PS substrates. PAH was first deposited onto the substrates, followed by the deposition of CNC-polymer bilayers. In the LbL fabrication process, alternating layers of CNCs and polymer (XG or PEI) were successively adsorbed from solution onto the substrates, forming one bilayer (N = 1). This bilayer deposition process was repeated to form films of varied thicknesses. The CNC-polymer films were then structured by heating the PS substrates, which caused them to shrink biaxially and wrinkle the CNC-polymer films. (b) Atomic force microscopy (AFM) height image of a structured CNC-polymer film composed of 20 bilayers (image zoomed into a flat area that allowed AFM tracing). (c) Chemical structures of xyloglucan and polyethyleneimine.

films into rough wrinkled surfaces with tuneable topographies that spanned the nano- to micrometer scale.

In addition to the final film thickness (dependent on N), LbL deposition parameters (type of polymer and polymer concentration) were varied to assess their impact on the morphology and mechanical properties of the CNC-polymer films before and after structuring. The polymer concentrations investigated were 0.1 wt% for films made with XG and PEI (labeled as CNC-$XG_{0.1}$ and CNC-$PEI_{0.1}$ films) and 1 wt% for PEI (labeled as CNC-$PEI_{1.0}$ films). Scanning electron microscopy (SEM) images of the structured nanobiocomposite films showed that the size of the wrinkles formed through shrinking increased as the number of deposited bilayers increased (Fig. 2), and were present across the whole film

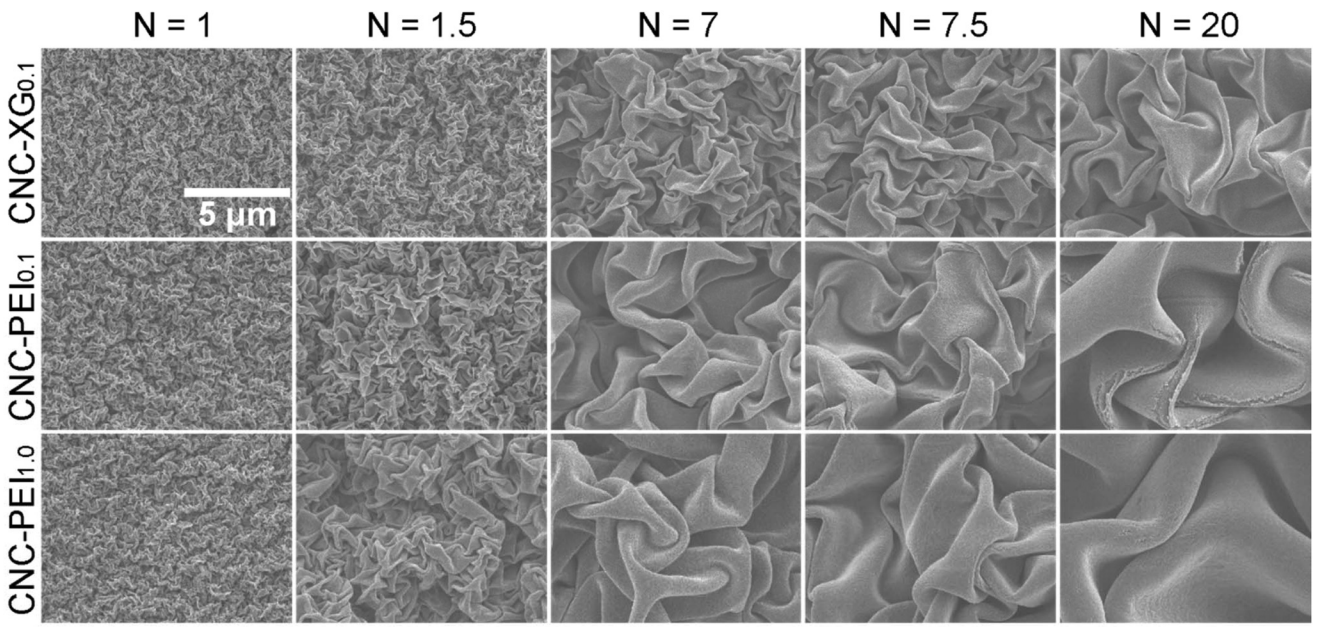

Fig. 2 SEM images of biaxially wrinkled CNC-polymer films with varying number of deposited bilayers.

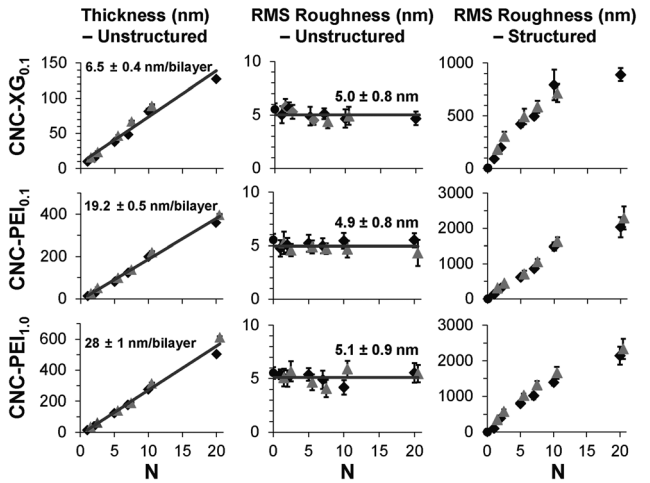

Fig. 3 Thickness measurements were obtained for all CNC-polymer films using variable angle spectroscopic ellipsometry, where the slopes indicate average thicknesses per bilayer in nanometers, n = 3, all $R^2 \geq 0.96$. White light interferometry was used to characterize the roughness of the nanobiocomposite films prior to structuring (lines and number indicate average roughness) and following structuring, $n \geq 15$. For all plots zero (•), full (◆) and half bilayers (▲) are indicated.

surface (1 × 1 cm). The increase in structure size suggested that the nanobiocomposite film thickness was proportional to the number of bilayers deposited (confirmed through ellipsometry measurements, *cf.* Fig. 3).

It is worth noting that films where the CNCs were the outermost layer (N + 0.5 bilayers) formed wrinkled features of comparable size to those formed with the additional polymer layer (N + 1 bilayers), indicating that the bulk of the film thickness arises from the addition of CNC layers. It was also observed that the nanobiocomposite films cracked at a lower number of layers when the outermost layer was made up of CNCs (Fig. S2†), which implies that the half bilayer film (N + 0.5) has a lower fracture toughness than the full bilayer one (N + 1). Film cracking was consistently observed throughout the wrinkled films when they contained more than 10 bilayers (Fig. 2 and S3†). These observations suggest that most of the film thickness and stiffness arises from the CNC layers, and that the polymer is a filler for the crevices left by the nanocrystals, where it acts as a plasticizer; it also suggests that there is a thickness beyond which the films can no longer accommodate the compressive stress generated, and fracture at the points of maximum strain (wrinkle ridges).

It was also observed that the amount of polymer incorporated played a significant role in the mechanics and structuring of the CNC-polymer films. A comparison between CNC-$PEI_{1.0}$ and CNC-$PEI_{0.1}$ films showed that the films prepared with the lower polymer concentration cracked at lower N, despite being thinner. This is evidence of PEI acting as a plasticizer, where increasing the polymer content in the film increased the film elasticity and effectively reduced the strain present within the films. Despite the cracking observed in thicker films, the structured CNC-polymer films were highly stable, as evidenced by the fact that they retained their integrity and structured morphology even after being lifted-off and transferred from the underlying PS substrate (Fig. S4†).

Characterization of CNC-polymer nanobiocomposite films

After establishing the shape-memory polymer shrinking as a reproducible and reliable method for structuring the CNC-polymer films and observing their unique characteristics, we evaluated their thickness and surface roughness as a function of film composition, polymer concentration, and composition of the outermost layer. Variable angle spectroscopic ellipsometry (VASE) measurements on unstructured films confirmed the linear correlation between N and film thickness (Fig. 3). However, it was observed that the thickness of the film remained relatively constant between films containing N + 0.5 and N + 1 bilayers. This confirmed our previous observation that CNCs are the main contributors to the film thickness and agrees with previous reports, where CNCs deposited onto flat surfaces from dilute suspensions resulted in open films with interstices between the nanoparticles that could be filled in and smoothed over by the subsequent addition of a polymer layer.[40,41] Thicker bilayers were obtained with higher polymer concentrations, as CNC-$PEI_{1.0}$ films exhibited thicker bilayers than CNC-$PEI_{0.1}$ films (28 ± 1 *vs.* 19.0 ± 0.5 nm per bilayer), and with PEI as the polymer layer over XG (19.0 ± 0.5 *vs.* 6.5 ± 0.4 nm per bilayer for CNC-$PEI_{0.1}$ and CNC-$XG_{0.1}$ films). The thickness per bilayer indicates that at least one layer of CNCs is adsorbing onto each polymer layer (given that CNCs have cross sections in the 5–10 nm range) and are consistent with previously reported thicknesses, which range from 6 to 39 nm per bilayer.[9,26,42–46]

The difference in bilayer thickness for films prepared from 0.1 wt% aqueous solutions of PEI *versus* XG can be attributed to the polymer structure and interaction with the CNCs. XG is known to adopt a flat linear conformation when deposited onto an underlying CNC layer,[29] which limits the total amount of polymer adsorbed and, subsequently, limits CNC adsorption. On the other hand, the branched and cationic nature of the deposited PEI allows the polymer chains to extend above the film surface, and increases its surface charge.[9] Electrostatic interactions cause a larger amount of CNCs to adsorb onto this layer, resulting in a thicker CNC layer and thus a thicker bilayer. The interactions between the polymer and CNC layers, and the ability to tune the thickness of the bilayers and the films can be translated into the fine tuning of the nanobiocomposite film mechanical properties and, ultimately, the size and periodicity of the structures fabricated through compressive stress.

White light interferometry microscopy measurements were used to assess the surface roughness of unstructured and structured CNC-polymer films. It was observed that while the film thickness increased with the number of layers present in the unstructured CNC-polymer films, their root mean squared (RMS) surface roughness remained constant at *ca.* 5 nm (Fig. 3) regardless of the outermost layer, film composition, or film thickness. These roughness values suggest that the topo-

graphy of the unstructured films was dominated by the widths of the CNCs and are similar to RMS roughness values previously reported for CNC-polymer films.[23,41,47] Following the shrinking of the shape-memory substrate, the topography of the structured CNC-polymer films became substantially rougher, where the roughness increased the thicker the films were (Fig. 3), with CNC-$PEI_{1.0}$ films exhibiting the largest RMS roughness for any given number of bilayers. In addition, it was observed that in most instances $N + 0.5$ bilayer films had RMS roughness values comparable to those of $N + 1$ bilayer films. This observation agrees with the notion that CNCs are the main contributors to the film thickness (Fig. 3) and structure size (*cf.* Fig. 2), and further suggests that the CNC layer is also the key component to determining the rigidity of the films. It was also observed that as N increased, particularly for the CNC-$XG_{0.1}$ films, the roughness plateaued and no increase in roughness was observed for films with additional bilayers (Fig. 3). The levelling-off of the surface roughness is attributed to the cracking observed in the films (*cf.* Fig. 2) and has previously been observed in oxide films with thicknesses >20 nm.[22] Thus, thicker films (larger N) cracked during the shrinking process to relieve strain and did not result in wrinkled features with ever-increasing size.

Mechanical properties and composition of CNC-polymer nanobiocomposite films

The elastic modulus of the different nanobiocomposite films was obtained in a humidity-independent way from the morphological data for the structured films and their corresponding thickness measurements. To this end, the periodicity in the topography of the wrinkled surfaces was quantified through 2D fast Fourier transform (2D FFT) analysis of SEM images (Fig. S1†). Intensity *vs.* characteristic length plots were generated (Fig. 4a and S1†) and the peaks with the highest intensity (inset box in Fig. 4a) were averaged to determine the characteristic wrinkle length (ζ) of the film. This quantity is proportional to the persistence length of the films ($\xi = a\zeta$), which represents the distance at which the wrinkle direction no longer recalls its original direction. Consistent with the film morphology (*cf.* Fig. 2) and roughness analysis (*cf.* Fig. 3), we observed that ζ increased linearly with film thickness (Fig. 4b–d). The elastic modulus was then determined by plotting the thickness (h) of the nanobiocomposite film *vs.* its characteristic wrinkle length (ζ). The theory describing these plots[33,34,48] relates ξ (and ζ) to h through the relation $\xi = 2\pi\eta^{2/3}h$, where η incorporates the elastic modulus and Poisson's ratio of the rigid film (E_f, ν_f) and the underlying substrate (E_{PS}, ν_{PS}). The scaling factor between ξ and ζ was estimated using gold as reference material. Thin gold films with thicknesses between 20–200 nm were structured, and the analysis was performed using reported values for the elastic modulus and Poisson's ratio of sputtered gold films and bulk polystyrene at 135 °C. Through this analysis, it was found that the scaling factor $a = 5.2 \pm 0.5$, which was used in all subsequent analysis for the nanobiocomposite films.

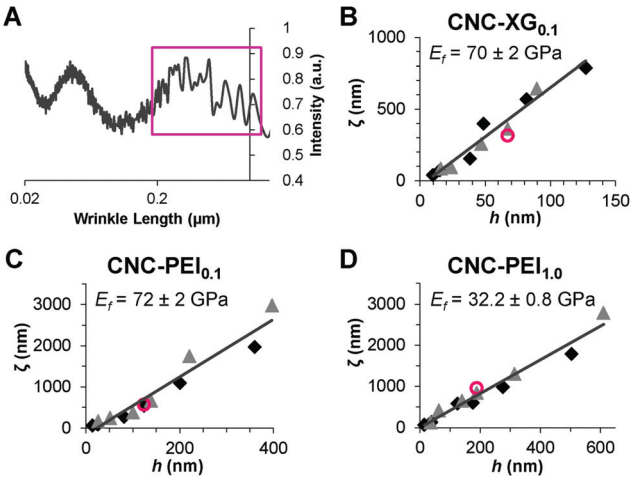

Fig. 4 Calculation of the elastic modulus from the morphological analysis of the structured nanobiocomposite films. (A) Intensity *versus* characteristic length plots were generated *via* 2D FFT analysis for the corresponding wrinkled structures. These plots were averaged, where the wrinkle length values at the highest intensities were determined (peaks in boxed area), and averaged to calculate the characteristic length. Plots of characteristic wrinkle length (ζ) *vs.* film thickness were generated for (B) CNC-$XG_{0.1}$, (C) CNC-$PEI_{0.1}$, and (D) CNC-$PEI_{1.0}$ films, where the slopes were used with eqn (1) to calculate the elastic moduli. Full (◆) and half (▲) bilayers are indicated, $n \geq 3$, all $R^2 > 0.94$–0.97. Open circles indicate films that were hydrated by immersion in water for 30 minutes prior to structuring.

The elastic moduli obtained for the CNC-polymer films through this morphological analysis were 70 ± 2 GPa (CNC-$XG_{0.1}$, Fig. 4b), 72 ± 2 GPa (CNC-$PEI_{0.1}$, Fig. 4c), and 32.2 ± 0.8 GPa (CNC-$PEI_{1.0}$, Fig. 4d). These values are reasonable given that the elastic modulus of a CNC-polymer film is dependent on its relative composition and on the interfacial interactions between the components, and that the reported elastic modulus for CNCs is in the 57–143 GPa range,[12,49] while PEI and XG have elastic moduli of 0.3 GPa[10] and 5.95 GPa,[50] respectively. Furthermore, the calculated values for the elastic modulus are in line with those previously reported for similar CNC-PEI LbL films, where the modulus was calculated as a function of relative humidity through the traditional SIEBIMM method.[9] We propose that our nanocomposites possess a larger modulus than those reported because most of the water entrapped in the films was removed during the shrinking step. To support this, we obtained identical morphology (elastic modulus) for films that were structured from a dry state and films that were fully hydrated (immersed in water for 30 minutes) prior to structuring (Fig. 4b–d, open circles). This shows that our structuring method is unaffected by the degree of hydration in the films and yields a value for the modulus that depends only on the intrinsic film composition.

It was interesting to note that significant differences in the mechanical properties of the nanobiocomposite films could be induced by simple changes in the film fabrication method, such as the type of polymer or polymer concentration used. This was attributed to the resulting film thickness (*cf.* Fig. 3)

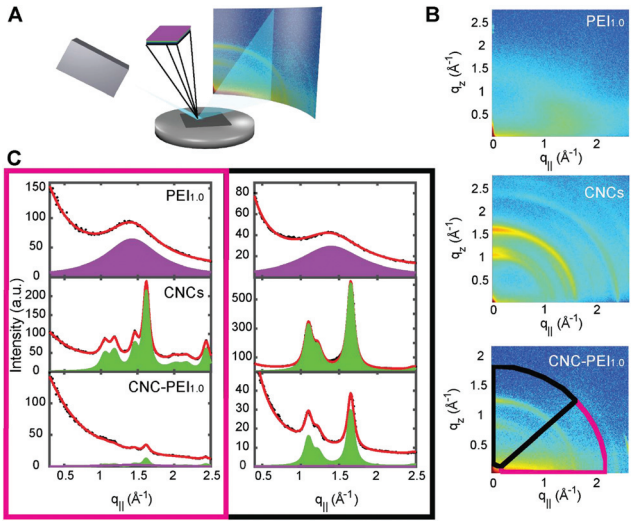

Fig. 5 X-ray diffraction measurements were used to determine the relative film compositions. (a) Schematic for the XRD set-up. (b) 2D X-ray plots in the *xy* plane ($q_{||}$) and *xz* plane (q_z) for pure polymer samples $PEI_{1.0}$ and CNCs, and a composite CNC-$PEI_{1.0}$ film (N = 20 bilayers). (c) Intensity data extracted from the 2D X-ray plot for the CNC-$PEI_{1.0}$ film was analyzed in two sections (black and pink outlines), and fitted using the X-ray profile obtained from the pure polymer samples.

and to the film's relative composition. The composition of the CNC-polymer films was determined using X-ray diffraction (XRD), where the scattering perpendicular (q_z) and parallel to the substrate surface ($q_{||}$) yielded characteristic 2-dimensional diffraction intensity patterns (Fig. 5a, b and S5–S7†). To extract the relative composition of the CNC-polymer nanocomposite films, base scattering functions were generated from pure CNC and pure polymer samples deposited through drop-casting. Then, a weighted sum of these functions was used to fit the scattering intensities of the films (Fig. 5c, S5 and S6†), where the relative weight of the function corresponded to the proportional mass of each component within the CNC-polymer film. The XRD methodology to calculate the nanobiocomposite film composition was validated using films prepared by drop-casting, where the solution contained CNC : $PEI_{1.0}$ at 50 : 50 composition by mass (Fig. S7†), and the calculated composition was 45 : 55.

The relative film compositions obtained through XRD analysis were 72 : 28 (CNC-$XG_{0.1}$), 82 : 18 (CNC-$PEI_{0.1}$), and 77 : 23 (CNC-$PEI_{1.0}$) CNC:polymer. In films fabricated with stock polymer solutions of the same weight percentage (0.1 wt%), films with PEI had a higher proportion of CNCs to polymer compared to XG. This compositional analysis matches the thicker bilayers and similar film stiffness observed for CNC-$PEI_{0.1}$ films over CNC-$XG_{0.1}$ films. Similarly, nanobiocomposite films fabricated from lower concentration PEI solutions (0.1 *vs.* 1 wt%) presented a higher CNC mass fraction, which correlates with the higher elastic modulus but not with thicker bilayers. Based on the observations for PEI-containing films, it can be concluded that the higher film stiffness was a result of the film proportion constituted by CNCs, and that this fraction decreased when more polymer was available to bind to the CNC layers. However, this could not be generalized for all nanobiocomposite films, as CNC-$XG_{0.1}$ films consisted of a lower proportion of CNCs to polymer but were significantly stiffer than CNC-$PEI_{1.0}$ films. The increased film modulus likely stems from the higher elastic modulus of XG (where it could be structured as a polymer-only film, Fig. S8a†), and its ability to crosslink individual layers of CNCs to form a stronger nanobiocomposite network with an increased stiffness, which would be akin to its role in crosslinking cellulose microfibrils in plant cell walls.[28,50–52]

From all the experiments combined, it is evident that CNCs are the key component that define the mechanical properties of the nanocomposite films, since they make up most of the film, contribute the majority of each bilayer thickness (*cf.* Fig. 3), provide the bulk of the rigidity (*cf.* Fig. 4), and thus are mainly responsible for the structuring of the thin film during compression. Yet the nature of the polymer and its interactions with cellulose are also important, since this strongly impacts the film, its rigidity, and ultimately its ability to buckle without fracturing, where CNC-only films readily crack under compressive stress (Fig. S8b†).

Conclusions

In this work, we have introduced a shape-memory polymer shrinking approach as a humidity-independent way to quantify the mechanical properties of CNC-polymer nanobiocomposite films, and obtained elastic modulus values that depend solely on nanobiocomposite film composition. To our knowledge, this is the first implementation of this structuring approach on nanobiocomposite thin films, and we have shown that the size, morphology, topography, and elastic modulus of the structured CNC-polymer films can easily be tuned through simple changes in the LbL deposition parameters (*i.e.*, type of polymer used, polymer concentration, and the number of deposited bilayers). The resulting structured biocomposites were found to be stable, irreversible, and reproducible, making them viable candidates for applications in sensor, packaging, or tissue engineering platforms. The elastic moduli calculated from the bionanocomposite films shows that the polymer identity and concentration during the film assembly process have a strong influence on its mechanical properties. The linear polymer xyloglucan can provide higher crosslinking interactions that result in films with high mechanical stiffness at lower thicknesses and CNC loading, compared to films assembled from a branched polycationic polymer. The technique presented here can be applied to evaluate the mechanical properties of a wide range of materials deposited through sputtering, chemical vapour deposition and evaporation, as well as through solvent and aqueous based deposition processes, and is particularly well suited for materials where humidity can have a large impact on the measured mechanical properties.

Acknowledgements

We thank S. Saem for help with scanning electron microscopy, E. Niinivaara for help with atomic force microscopy, and P. Mascher and J. Wojcik for access to VASE instrumentation, training on measurements, and analysis. UG is the recipient of an Ontario Graduate Scholarship, and JMM and EDC are recipients of Early Researcher Awards from the Ontario Ministry of Research and Innovation. This research was supported by funding through the Natural Sciences and Engineering Research Council and made use of instrumentation from the McMaster Manufacturing Research Institute, Canadian Centre for Electron Microscopy, Brockhouse Institute for Materials Research, Biointerfaces Institute, and the Centre for Emerging Device Technology.

References

1 B. Rogers, S. Pennathur and J. Adams, *Nanotechnology: Understanding Small Systems*, CRC Press, Boca Raton, FL, 2nd edn, 2011.
2 G. Cao and Y. Wang, *Nanostructures and Nanomaterials: Synthesis, Properties and Applications*, World Scientific, Singapore, 2nd edn, 2011.
3 X. Xu, L. Heng, X. Zhao, J. Ma, L. Lin and L. Jiang, *J. Mater. Chem.*, 2012, **22**, 10883–10888.
4 L. Heng, X. Guo, T. Guo, B. Wang and L. Jiang, *Nanoscale*, 2016, **8**, 13507–13512.
5 *Front Matter, in Polymer Composites*, ed. S. Thomas, K. Joseph, S. K. Malhotra, K. Goda and M. S. Sreekala, Wiley-VCH Verlag GmbH & Co. KGaA, Weinheim, Germany, 2013, Vol. 2.
6 C. M. Stafford, C. Harrison, K. L. Beers, A. Karim, E. J. Amis, M. R. VanLandingham, H.-C. Kim, W. Volksen, R. D. Miller and E. E. Simonyi, *Nat. Mater.*, 2004, **3**, 545–550.
7 C. Aulin, S. Ahola, P. Josefsson, T. Nishino, Y. Hirose, M. Österberg and L. Wågberg, *Langmuir*, 2009, **25**, 7675–7685.
8 R. J. Moon, A. Martini, J. Nairn, J. Simonsen and J. Youngblood, *Chem. Soc. Rev.*, 2011, **40**, 3941–3994.
9 K. H. M. Kan and E. D. Cranston, *Tappi J.*, 2013, **12**, 9–17.
10 E. D. Cranston, M. Eita, E. Johansson, J. Netrval, M. Salajková, H. Arwin and L. Wågberg, *Biomacromolecules*, 2011, **12**, 961–969.
11 M. Roman, *Ind. Biotechnol.*, 2015, **11**, 25–33.
12 Y. Habibi, L. A. Lucia and O. J. Rojas, *Chem. Rev.*, 2010, **110**, 3479–3500.
13 S. J. Eichhorn, A. Dufresne, M. Aranguren, N. E. Marcovich, J. R. Capadona, S. J. Rowan, C. Weder, W. Thielemans, M. Roman, S. Renneckar, W. Gindl, S. Veigel, J. Keckes, H. Yano, K. Abe, M. Nogi, A. N. Nakagaito, A. Mangalam, J. Simonsen, A. S. Benight, A. Bismarck, L. A. Berglund and T. Peijs, *J. Mater. Sci.*, 2010, **45**, 1–33.
14 R. R. Lahiji, X. Xu, R. Reifenberger, A. Raman, A. Rudie and R. J. Moon, *Langmuir*, 2010, **26**, 4480–4488.
15 A. Šturcová, G. R. Davies and S. J. Eichhorn, *Biomacromolecules*, 2005, **6**, 1055–1061.
16 Y. Cao, P. Zavattieri, J. Youngblood, R. Moon and J. Weiss, *Constr. Build. Mater.*, 2016, **119**, 71–79.
17 C. M. Stafford, S. Guo, C. Harrison and M. Y. M. Chiang, *Rev. Sci. Instrum.*, 2005, **76**, 62207.
18 C. M. Gabardo, Y. Zhu, L. Soleymani and J. M. Moran-Mirabal, *Adv. Funct. Mater.*, 2013, **23**, 3030–3039.
19 S. Lin, E. K. Lee, N. Nguyen and M. Khine, *Lab Chip*, 2014, **14**, 3475–3488.
20 S. Sonney, N. Shek and J. M. Moran-Mirabal, *Biomicrofluidics*, 2015, **9**, 26501.
21 S.-J. Park, J. Kim, M. Chu and M. Khine, *Adv. Mater. Technol.*, 2016, **1**, 1600053.
22 Y. Zhu, J. Boyle, K. Bonin, T. Chowdhury and J. M. Moran-Mirabal, Unpublished Data.
23 B. Jean, L. Heux, F. Dubreuil, G. Chambat and F. Cousin, *Langmuir*, 2009, **25**, 3920–3923.
24 C. Aulin, I. Varga, P. M. Claesson, L. Wågberg and T. Lindström, *Langmuir*, 2008, **24**, 2509–2518.
25 N. C. Carpita and D. M. Gibeaut, *Plant J.*, 1993, **3**, 1–30.
26 C. Cerclier, A. Guyomard-Lack, C. Moreau, F. Cousin, N. Beury, E. Bonnin, B. Jean and B. Cathala, *Adv. Mater.*, 2011, **23**, 3791–3795.
27 A. Guyomard-Lack, C. Cerclier, N. Beury, B. Jean, F. Cousin, C. Moreau and B. Cathala, *Eur. Phys. J.: Spec. Top.*, 2012, **213**, 291–294.
28 C. Cerclier, F. Cousin, H. Bizot, C. Moreau and B. Cathala, *Langmuir*, 2010, **26**, 17248–17255.
29 A. Villares, C. Moreau, A. Dammak, I. Capron and B. Cathala, *Soft Matter*, 2015, **11**, 6472–6481.
30 A. Dammak, C. Moreau, F. Azzam, B. Jean, F. Cousin and B. Cathala, *J. Colloid Interface Sci.*, 2015, **460**, 214–220.
31 J.-F. Revol, H. Bradford, J. Giasson, R. H. Marchessault and D. G. Gray, *Int. J. Biol. Macromol.*, 1992, **14**, 170–172.
32 T. Abitbol, E. Kloser and D. G. Gray, *Cellulose*, 2013, **20**, 785–794.
33 J. Groenewold, *Physica A*, 2001, **298**, 32–45.
34 F. Greco, A. Bellacicca, M. Gemmi, V. Cappello, V. Mattoli and P. Milani, *ACS Appl. Mater. Interfaces*, 2015, **7**, 7060–7065.
35 M. C. Salvadori, I. G. Brown, A. R. Vaz, L. L. Melo and M. Cattani, *Phys. Rev. B: Condens. Matter*, 2003, **67**, 153404.
36 T. C. Hodge, S. A. Bidstrup-allen and P. A. Kohl, *IEEE Trans. Compon., Packag., Manuf. Technol., Part A*, 1997, **20**, 241–250.
37 P. H. Mott, J. R. Dorgan and C. M. Roland, *J. Sound Vib.*, 2008, **312**, 572–575.
38 E. Chanliaud, K. M. Burrows, G. Jeronimidis and M. J. Gidley, *Planta*, 2002, **215**, 989–996.
39 M. Shir Mohammadi, C. Hammerquist, J. Simonsen and J. A. Nairn, *J. Mater. Sci.*, 2016, **51**, 8916–8927.
40 E. Kontturi, L.-S. Johansson, K. S. Kontturi, P. Ahonen, P. C. Thüne and J. Laine, *Langmuir*, 2007, **23**, 9674–9680.
41 E. D. Cranston and D. G. Gray, *Biomacromolecules*, 2006, **7**, 2522–2530.

42 L. Sui, L. Huang, P. Podsiadlo, N. A. Kotov and J. Kieffer, *Macromolecules*, 2010, **43**, 9541–9548.
43 E. D. Cranston and D. G. Gray, *Sci. Technol. Adv. Mater.*, 2006, **7**, 319–321.
44 E. D. Cranston, D. G. Gray and M. W. Rutland, *Langmuir*, 2010, **26**, 17190–17197.
45 P. Podsiadlo, S.-Y. Choi, B. Shim, J. Lee, M. Cuddihy and N. A. Kotov, *Biomacromolecules*, 2005, **6**, 2914–2918.
46 A. Dammak, C. Moreau, N. Beury, K. Schwikal, H. T. Winter, E. Bonnin, B. Saake and B. Cathala, *Holzforschung*, 2013, **67**, 579–586.
47 C. D. Edgar and D. G. Gray, *Cellulose*, 2003, **10**, 299–306.
48 C.-C. Fu, A. Grimes, M. Long, C. G. L. Ferri, B. D. Rich, S. Ghosh, S. Ghosh, L. P. Lee, A. Gopinathan and M. Khine, *Adv. Mater.*, 2009, **21**, 4472–4476.
49 M. Mariano, N. El Kissi and A. Dufresne, *J. Polym. Sci., Part B: Polym. Phys.*, 2014, **52**, 791–806.
50 J. Kochumalayil, H. Sehaqui, Q. Zhou and L. A. Berglund, *J. Mater. Chem.*, 2010, **20**, 4321–4327.
51 J. J. Kochumalayil and L. A. Berglund, *Green Chem.*, 2014, **16**, 1904–1910.
52 T. Hayashi and R. Kaida, *Mol. Plant.*, 2011, **4**, 17–24.